 ©2010 Kvantovaya Elektronika and Turpion Ltd

LASER PLASMA

PACS numbers: 52.50.Jm; 52.70.Kz; 52.72+v
DOI: 10.1070/QE2010v040n10ABEH014285

Investigation of the optical characteristics of a laser-produced plasma cloud expanding into a background gas

A.I. Annenkov, A.V. Bessarab, I.V. Galakhov, S.G. Garanin, A.V. Gusakov, N.V. Zhidkov, V.A. Zhmailo, V.M. Izgorodin, V.P. Kovalenko, V.A. Krotov, V.V. Mis'ko, E.A. Novikova, V.A. Starodubtsev, K.V. Starodubtsev, V.P. Statsenko, R.R. Sungatullin, G.V. Tachaev, Yu.N. Sheremet'ev

***Abstract*. An investigation is made of the dynamics and visible-range luminosity of the plasma cloud produced behind the front of a shock wave in air at a pressure of 1 Torr. The shock wave was produced on introducing the radiation of the twelve-channel Iskra-5 laser facility with a total energy of ~ 2300 J into a hollow spherical plastic target of mass $\sim 10^{-4}$ g. Experimental data are compared with simulations.**

Keywords: *laser-produced plasma, shock wave in background gas, spatio-temporal dynamics of luminosity*.

1. Introduction

Bogunenko et al. [1] and Atamanenko et al. [2] investigated the development of a luminous plasma domain (LPD) emerging in the atmosphere of a vacuum chamber in the evaporation and expansion of a laser target. These experiments were staged in the MKV-4 chamber accommodated in one of the channels of the Iskra-5 laser facility [3]. The energy liberation in a target of mass $\sim 10^{-4}$ g achieved in the experiments amounted to several hundred joules for a pressure of ~ 1 Torr in the chamber (the air). For these parameters, in the LPD it is possible to obtain a variety of physical processes which are seldom the case in plasma physics. First and foremost, we have to do with kinetic and radiation transfer processes. Furthermore, the expansion dynamics of the target and its interaction with the 'atmosphere' are such that experiments of this kind turn out to be an important means of testing physical models and numerical techniques [4, 5], which in turn may be employed [6, 7] for the simulation of transient astrophysical and geophysical phenomena. These circumstances gave impetus to the pursuance of the experiments outlined in Refs [1, 2] as well as in the present paper.

The main difference of our experiments from those described in Refs [1, 2] consists in a substantial (by nearly an order of magnitude) increase in the energy of a laser pulse introduced into the target. This enabled us to reveal the influence of this parameter on LPD properties as well as to test the techniques [4, 5] mentioned above in a wider range of LPD parameter variation. These were the objectives of our work.

In addition to the data of simulations intended to perform a comparison with experimental data, in this work we give the simulation data for several LPD characteristics which eluded measurement. These data enable acquiring more comprehensive information about the processes that govern the LPD development.

A.I. Annenkov, A.V. Bessarab, I.V. Galakhov, S.G. Garanin, A.V. Gusakov, N.V. Zhidkov, V.A. Zhmailo, V.M. Izgorodin, V.P. Kovalenko, V.A. Krotov, V.V. Mis'ko, E.A. Novikova, V.A. Starodubtsev, K.V. Starodubtsev, V.P. Statsenko, R.R. Sungatullin, G.V. Tachaev, Yu.N. Sheremet'ev Russian Federal Nuclear Centre 'All-Russian Research Institute of Experimental Physics', prosp. Mira 37, 607190 Sarov, Nizhnii Novgorod region, Russia;
e-mail: starodub@otd13.vniief.ru

Received 20 January 2010; revision received 2 August 2010
Kvantovaya Elektronika **40** (10) 873 – 878 (2010)
Translated by E.N. Ragozin

2. Formulation of experiments

Experiments aimed at measuring the optical characteristics of an LPD emerging under the action of a shock wave (SW) in the atmosphere of the background gas were carried out in a spherical interaction chamber 2 m in diameter. The LPD emerged when the second harmonic ($\lambda = 0.66$ μm) of the radiation of twelve channels of the Iskra-5 iodine laser [3] was introduced into a hollow spherical plastic target of diameter 3.2 mm and mass 10^{-4} g with six openings ~ 600 μm in diameter. The radiation of two laser channels was simultaneously introduced through each opening. The total laser energy E_{las} delivered to the target was equal to 2300 J for an integral pulse duration of 0.5 ns; the background air pressure in the chamber was equal to 1 Torr.

To investigate the SW formation and propagation, the dynamics and optical characteristics of the LPD, advantage was taken of the following techniques:

(i) The technique of measuring the LPD radiation flux in the 0.32 and 0.45 μm spectral ranges by means of coaxial photocells and photodiodes. The spectral selection of radiation was effected by colour filters.

(ii) Recording the spatio-temporal characteristics of the glow of the plasma cloud (PC) in the visible range (0.35 – 0.5 μm) using streak cameras operating in frame- and slit-scan modes [8].

3. Formulation of numerical simulations

To interpret the resulting experimental data, use was made of the physical model and SNDP numerical technique described by Dolgoleva [4] and Dolgoleva and Bel'kov [5]. The model included the following physical processes: two-temperature gas dynamics, spectral radiation transfer, radiation – matter interactions, as well as electron and ion

thermal conduction. The nonequilibrium composition of the medium was calculated by the average-ion model.

Our simulations were performed in the spherical geometry. The numerical technique was one-dimensional and Lagrangian. The gas-dynamic equations were solved using a completely conservative implicit scheme. The target material was treated as a mixture of C and H atoms (in the 1 : 1 proportion) and the atmosphere (the air) as a mixture of N and O atoms (in the standard proportion). The existence of molecular components in the air plasma was neglected (our estimates made using the calculated values of the LPD temperature and density confirm the validity of this approximation for the LPD development stage considered in our work).

The absorption of laser pulses was calculated according to the model of Bel'kov et al. [9]. The radiation transfer was calculated using the multigroup spectral diffusion (38 groups) or quasidiffusion approximations [4]. The validity of this approximation to the problem under consideration is confirmed by our simulations data, which suggest (see below) that the LPD is optically thin and the above approximation therefore provides the correct passage to the limit of exact solution for the radiation flux [10].

Imposed at the outer boundary were the condition of free radiation escape and the 'rigid wall' condition for gas-dynamic equations.

4. Results of experiments and simulations

4.1 Dynamics of plasma cloud expansion

In our experiments, measurements were made of PC brightness profile with the aid of streak cameras operating in the slit scan and frame recording modes. In both cases the spectral range of recording covered the 0.35-to-0.5 μm wavelength range. The slit width of the streak camera photocathode was ~ 70 μm, corresponding to a spectral resolution of 110 ns.

Figures 1 and 2 show the results of recording the PC luminosity (I) obtained with the help of streak cameras in the frame and slit scan modes, respectively. In the first five frames in Fig. 1 there occurred photocathode saturation (its dynamic range is 8 bits) at the centre of the LPD. That is why only the points in time corresponding to the last four frames were taken into account in the analysis of luminosity profiles.

Figure 3 shows the results of experimental data processing in the form of $R - t$ diagrams for the boundary of PC luminosity at a level corresponding to the ratio between the boundary luminosity I_{th} and the peak luminosity $I_{\max}$, $\varepsilon = I_{\text{th}}/I_{\max} = 0.1$, in the optical range for an experiment with an energy input of 2300 J. Also shown in Fig. 3 are the simulation data for $\varepsilon = 0.03$ and 0.1, which are in good agreement with experimental data. One can see that the calculated LPD radius defined by the level $\varepsilon = 0.03$ increases monotonically, which is consistent with experimental data obtained with the streak camera in the slit scan mode. With increasing ε up to 0.1, at some point in time it begins to shorten, which is in agreement with the data of the frame recorder.

Similar data obtained in experiments with an energy input of 300 J on the MKV-4 facility are given for comparison in Fig. 4.

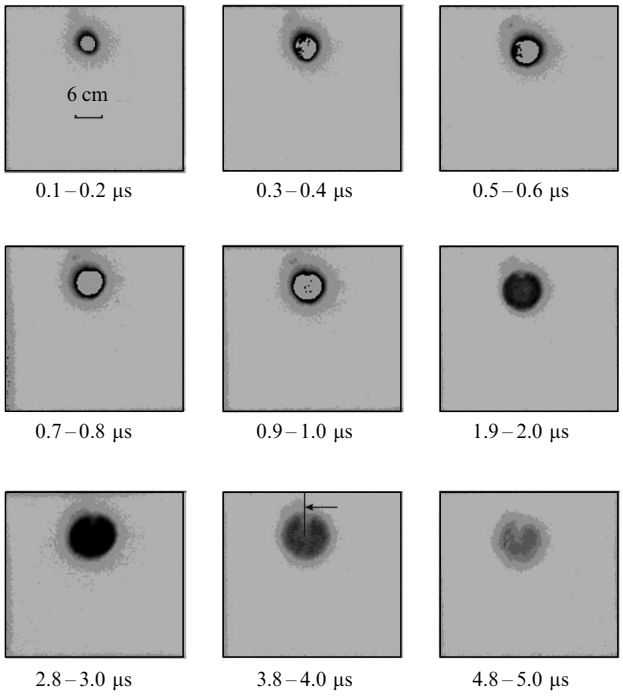

Figure 1. Result of frame recording of PC luminosity (the arrow indicates the location of target suspension).

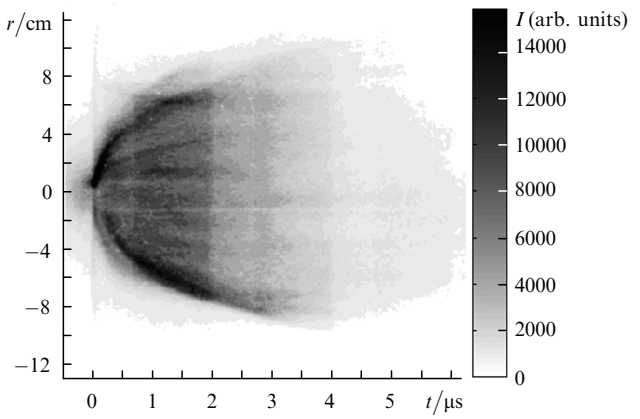

Figure 2. Slit scan of PC luminosity (the time origin corresponds to the arrival of a laser pulse, the radius origin corresponds to the initial target location).

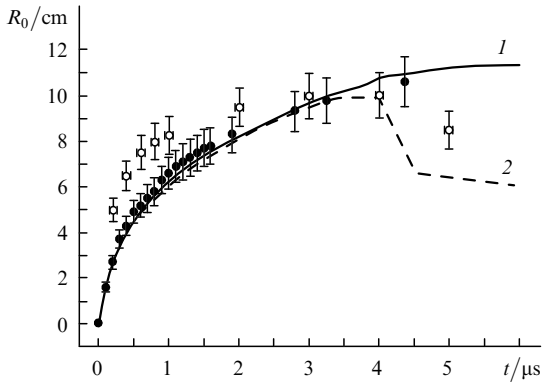

Figure 3. $R - t$ diagrams of the PC luminosity boundary for a laser pulse energy of 2300 J: simulation data for $\varepsilon = 0.03$ (*1*) and 0.1 (*2*); measurement data obtained using the frame (○) and slit scan (●) modes.

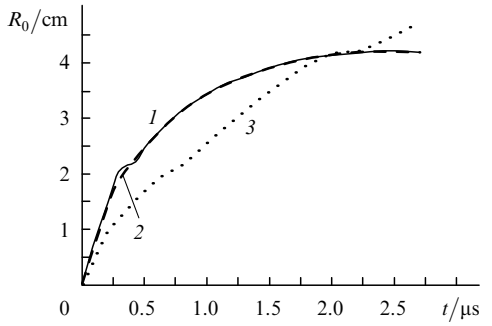

Figure 4. $R-t$ diagrams of the PC luminosity boundary in experiments with a laser radiation energy of 300 J in the spectral region $\lambda = 0.45$ μm: simulation data for $\varepsilon = 0.03$ (*1*) and 0.1 (*2*); measurement data obtained using a frame recorder (3).

4.2 Brightness profiles of the plasma domain

The expression for spectral brightness B_ν may be written in the form of an integral along the chord normal to the radius:

$$B_\nu(r) = \int_{-s_{\max}(r)}^{s_{\max}} I_\nu(r') \exp\left[-\int_s^{s_{\max}} \kappa_\nu(r'')\mathrm{d}s'\right]\mathrm{d}s, \qquad (1)$$

where

$$I_\nu(r) = \frac{1}{r^2}\frac{\partial S_\nu}{\partial r}; \qquad (2)$$

$$r' = \sqrt{r^2 + s^2}; \quad r'' = \sqrt{r^2 + s'^2}. \qquad (3)$$

In these formulas use was made of the quantities $S_\nu(r)$ (the total radiation flux in the spectral range under consideration) and κ_ν (the spectral absorption coefficient), which were calculated employing the SNDP technique. We emphasise that relationships (1)–(3) are the exact solution of the radiation transfer equation rather than the diffusion one (see Section 3).

The PC brightness profiles are plotted in Figs 5 and 6 for different points in time. The experimental data given in these drawings are so normalised that their peak values coincide with the calculated ones. The impression about the agreement between our simulations and experiments as regards absolute brightness can gained from Fig. 7 (see below).

Referring to Fig. 5, one can see that the experimental curves show oscillations of the PC brightness located between the extreme peaks, which is not observed in our simulations. Evidently these oscillations are due to the fact that the laser radiation is introduced into the target through openings and the brightness in their vicinity exceeds the brightness of the remaining LPD. As seen from Fig. 5, the brightness profiles measured by the streak camera in the slit scan mode at the initial stage are more blurred than the calculated ones. This supposedly testifies to departures from one-dimensionality (from spherical symmetry) at this stage. Indeed, the departure from one-dimensionality should weaken with increasing LPD dimensions (this is so when long radial distances are involved, this is not the case for the central part). That is why, as is evident from the drawings, the calculated brightness profiles approach the measured ones for later points in time. This is also borne out by Fig. 6, which compares our simulations with the data measured by the frame recorder at later points in time. As Fig. 6 suggests, by and large these results are close to each other.

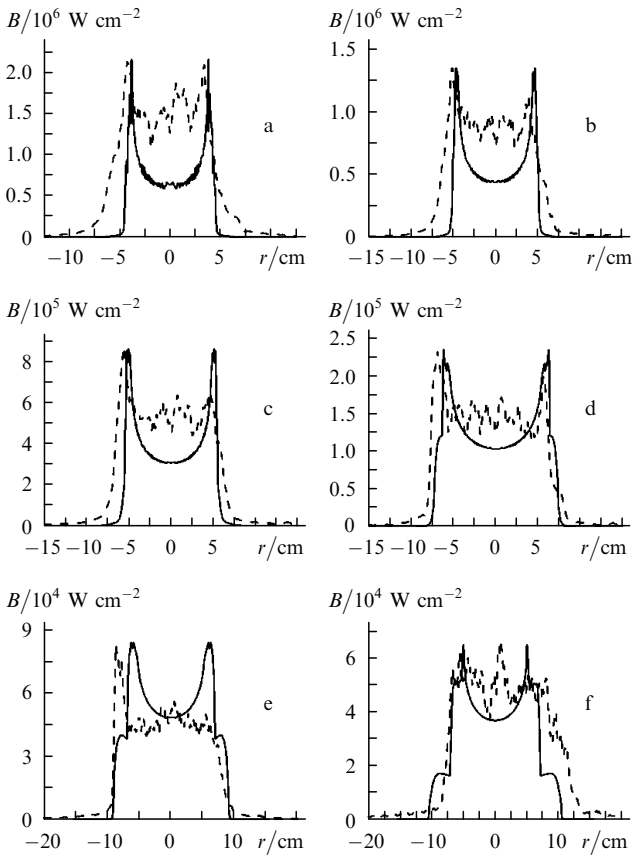

Figure 5. Comparison of the calculated PC brightness profiles (solid curves) with the data obtained using the streak camera in the slit scan mode (dashed curves) at the points in time $t = 0.45$ (a), 0.65 (b), 0.85 (c), 1.5 (d), 2.5 (e), and 3.6 μs (f).

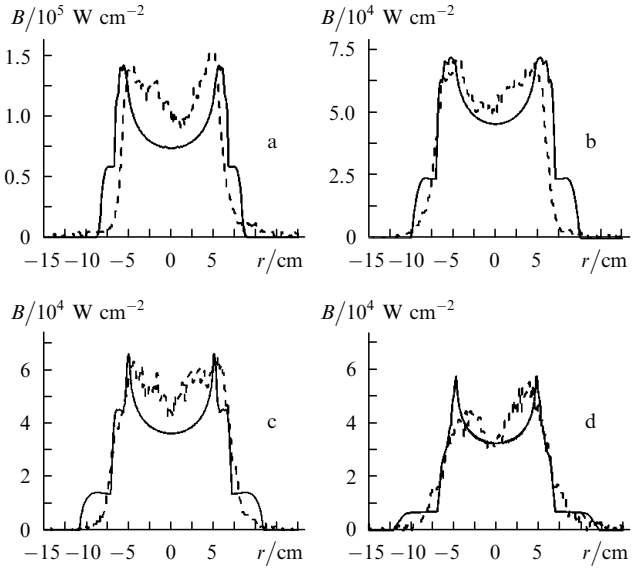

Figure 6. Comparison of the calculated PC brightness profiles (solid curves) with those measured using the frame recorder (dashed curves) at the points in time $t = 1.95$ (a), 2.9 (b), 3.9 (c), and 5.3 μs (d).

4.3 Spectral-temporal dependences of the plasma domain radiation intensity

Figure 7 shows the time dependences of the plasma radiation flux in the near-UV and blue spectral domains, which were measured in experiments with an in-target

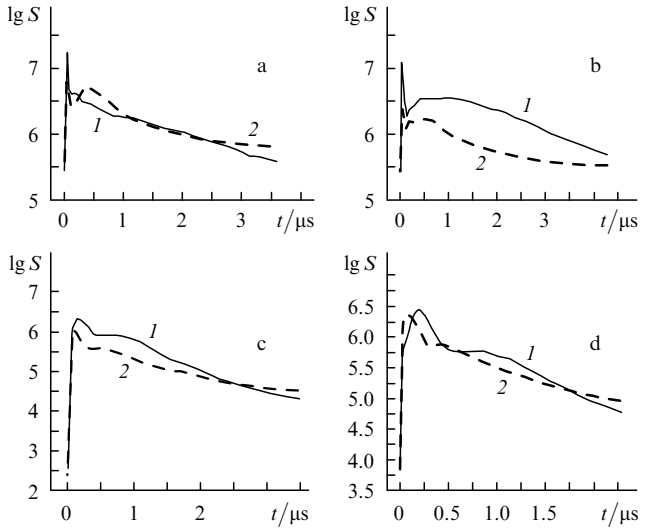

Figure 7. Time dependences of the total PC radiation flux (in W sr^{-1} μm^{-1}) in the spectral domains near 0.32 μm (a, d) and 0.45 μm (b, c) for experiments of 10.04.08 (a, b; $E_{las} = 2300$ J) and 18.03.08 (c, d; $E_{las} = 300$ J): (*1*) experiment; (*2*) simulations.

energy liberation $E_{las} = 2300$ J and obtained from simulations using the SNDP technique. Also given for comparison are the measurement data for an energy liberation $E_{las} = 300$ J performed using the MKV-4 facility.

As is evident from Fig. 7, for $t \leqslant 3$ μs the data of simulations and measurements are in satisfactory agreement for both spectral domains.

Comparative data on the integral LPD characteristics in the 0.35–0.50 μm spectral range for energies $E_{las} = 0.3$ and 2.3 kJ are collected in Table 1. The tabulated data suggest that the increase in E_{las} resulted primarily in an increase of LPD surface area and a lengthening of LPD glow duration. A more comprehensive and detailed picture of LPD development may be obtained by invoking the results of additional simulations.

Table 1. Integral LPD characteristics.

E_{las}/kJ	Radiated energy/J	Radiation pulse duration/μs	LPD size at the point in time $t = 5$ μs/cm
0.3	3–4	0.5	3–4
2.3	10–12	1.0	8–10

5. Results of the simulations of dynamics, kinetics, and radiation transfer in the LPD

The main parameters characterizing the dynamics of LPD development are as follows: the energy (E_{las}) of a laser pulse inputted into the target, the target mass (M), the atmospheric pressure and density (p and ρ, respectively). Using these quantities it is possible to form characteristic lengths

$$\mathscr{R} = \left(\frac{3M}{4\pi\rho_0}\right)^{1/3} \quad \text{and} \quad R = \left[\frac{3(\gamma^2-1)E_{las}}{8\pi p_0(3\gamma-1)}\right]^{1/3},$$

as well as velocities

$$u = \sqrt{E_{las}/M} \quad \text{and} \quad c_0 = \sqrt{\gamma p_0/\rho_0}.$$

Here, $\mathscr{R}$ is the target material (TM) deceleration radius; R is the radius of the shock front; u is the TM expansion velocity; and c_0 is the sound velocity in the chamber atmosphere. In the context of our experiment, $\mathscr{R} = 3$ cm, $R = 3$ m, $u = 1.5 \times 10^7$ cm s^{-1}. We note that the free paths of the photons with energies of 20, 200, 500, and 1000 eV in the 'cool' atmosphere of the chamber is equal to 10, 100, 300, and 500 cm, respectively [10].

By comparing these values with the characteristic LPD dimensions and the LPD observation times introduced above, one may draw an inference that our observations cover two stages of LPD development: the stage of energy transfer from the TM to the atmosphere by way of radiation and gas-dynamic deceleration of the TM ($t < t_1 = \mathscr{R}/u = 0.1$ μs) and the stage of a strong point explosion ($t_1 < t < t_2$, where $t_2 = R/c_0 = 10^{-2}$ s).

The bulk of radiation from the target is emitted in the X-ray range (1 keV photon energy) in a time $t < 0.01$ μs. An energy of 0.5 kJ is radiated during this period. The radiated energy is absorbed in a domain of radius roughly equal to the X-ray photon free path in the chamber atmosphere. For the given pressure, the free path is ~ 1 m. The absorption leads to atmospheric ionisation and heating. The profiles of the electron temperature T_e and ion multiplicity z are plotted in Fig. 8. Referring to Fig. 8, effects caused by the X-ray radiation (XRR) from the target are seen at distances r greater than 1–2 cm.

By the point in time $t = 0.01$ μs there occurred thermalisation of photoelectrons (due to the ionisation and excitation of atoms). The resultant electron temperature and density profiles are determined by the development of electron avalanche for a given (at each point) XRR energy

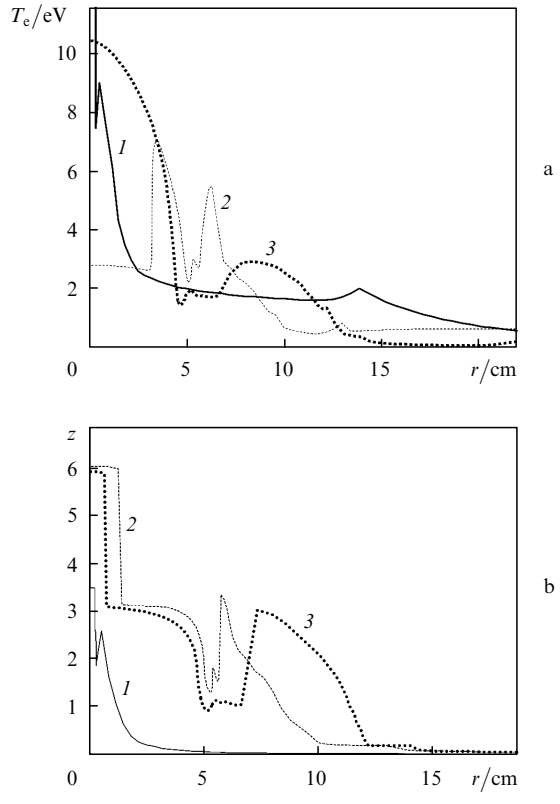

Figure 8. Profiles of the electron temperature (a) and ion multiplicity (b) for experiments with $E_{las} = 2300$ J for $t = 0.01$ (*1*), 1 (*2*), and 5 μs (*3*).

liberation. In this case, $T_e \approx$ const and $z \sim E_{las}/r^2$, which is reflected in Fig. 8 [curves (*1*)]. In particular, the radius of the domain where $z \geqslant 0.01$ is equal to ~ 15 cm for $E_{las} = 2.3$ kJ and to ~ 5 cm for $E_{las} = 0.3$ kJ. In this case, our simulations suggest that away from the SW front there holds an inequality.

For distances r shorter than 3–5 cm there prevail perturbations arising from the SW formation due to the expansion of the TM. By the point in time under consideration the free expansion of the TM has already developed and the deceleration may still be neglected. The position of the TM boundary [to this position there corresponds a dip in curve (*1*) for $r = 0.3$ cm in Fig. 8b] is consistent with the velocity u given above. Adjacent to this boundary is the SW front; the atmospheric layer ahead of the front is appreciably heated and ionised by the UV radiation from the front (where $T_e \sim 10 - 30$ eV). Here is the onset of the formation of a structure corresponding to the front structure of a supercritical-amplitude SW [10].

Subsequently the LPD development is governed primarily by gas dynamics; for $t > 0.1$ μs, when $R > \mathscr{R}$, one can see transition to the stage of a strong point explosion. This is clearly seen from the comparison of curves (*2*) and (*4*) in Figs 9a and 9b, which represent $R - t$ diagrams characterising the processes under discussion for $E_{las} = 0.3$ and 2.3 kJ, respectively. The former curve is the radius of the SW front (R) obtained in our simulations. The latter curve is the SW front radius obtained in the framework of the theory of a strong (Sedov) explosion with the use of the parameter ξ_0 (see Zel'dovich and Raizer [10]) corresponding to a value $\gamma = 1.24$ recommended in Ref. [10].

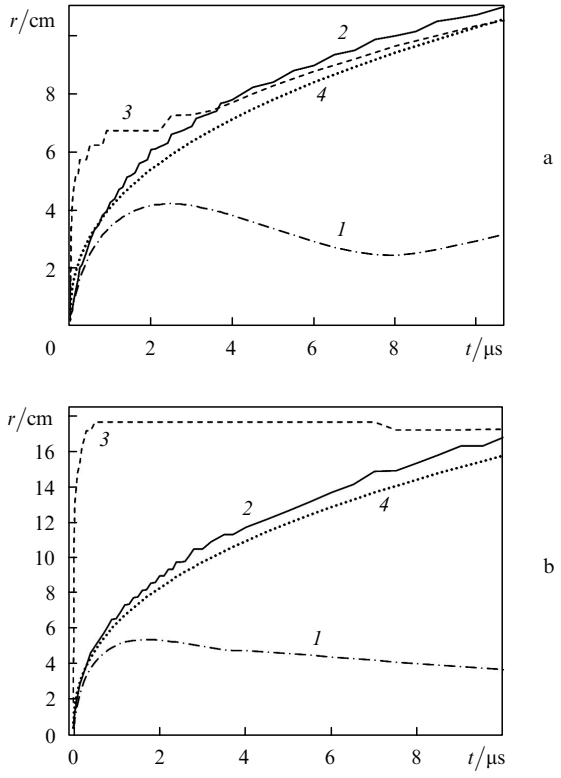

Figure 9. $R - t$ diagram at $E_{las} = 300$ (a) and 2300 J (b): (*1*) radius of TM deceleration; (*2*) radius of the UV front; (*3*) radius of points r_{ion}, where the background ionisation multiplicity is reached (~ 0.01); (*4*) Chernyi's approximate solution [10].

For a more detailed elucidation of the roles of radiation and nonequilibrium character of kinetic processes, we performed a gas-dynamic simulation with the inclusion of equilibrium real equations of state of the air [11]. The results of this simulation with respect to R coincide with the results represented in Fig. 9 [curves (*2*)].

This coincidence is consistent with the fact that the radiation and the nonequilibrium character of kinetics behind the SW front do not exert appreciable effects on the processes for the given atmospheric density. Indeed, for the values of temperature [see curves (*1–3*) in Fig. 8a] and density characteristic for this domain, Planck paths $l_p > 103$ cm $\gg R$. Therefore, the plasma under consideration is optically thin. Furthermore, a comparison of the profiles of ion multiplicity z [see curves (*1–3*) in Fig. 8b] with those calculated in the equilibrium approximation for the temperature (Fig. 8a) and density behind the SW front reveals not only their mutual qualitative agreement, but their quantitative agreement as well.

These circumstances permit invoking the strong-explosion theory (with the inclusion of a finite target mass) to interpret our experimental data. In doing this, we assume the LPD to be optically thin.

We begin with the data on the dependence of LPD dimensions (R_0) on the energy E_{las} and time t, which are given in Figs 3 and 4. Comparing these dimensions with the data on R (Fig. 9) shows their close proximity. [This proximity is natural, since the ion multiplicity $z > 1$ everywhere behind the SW front at the points in time under consideration (see Fig. 8b).] Therefore, the sought-for dependences are defined by the known formulas for R. The same formulas determine the R_0 values in Table 1. We note that the lag of R_0 relative to R becomes noticeable for $t > 10$ μs.

As regards the brightness profiles shown in Figs 5 and 6, we note that the positions of the front in all of the curves coincide with the calculated position of the SW front. In the domain behind the SW front there are peaks whose location corresponds to the radius of the atmospheric layer wherein the ion multiplicity is highest (see Fig. 8b). This circumstance may be interpreted proceeding from the behaviour of temperature and density profiles behind the SW in the strong-explosion theory and the Kramers–Unsold model for plasma radiation capacity [10]. It is pertinent to note that the TM contribution to the calculated brightness is negligible for $t > 1$.

Figure 10 gives the results of calculation of the temporal variation of total-energy components for the problem involved. As is seen from the drawing, by the point in time $t = 5$ μs the radiated energy fraction is equal to 1/25 and 1/10 of the total energy for $E_{las} = 0.3$ and 2.3 kJ, respectively. We emphasise that in the latter case a significant (~ 0.5) contribution to this energy is made by the initial radiation from the target (see Fig. 10b). Should we proceed from estimates based on the theory mentioned above, the corresponding values would be $\sim 1/15$ and 1/10. Hence, we may draw a conclusion that this theory yields reasonable estimates for the radiated energy.

As regards nonequilibrium effects of radiation and kinetics at the stage of a point explosion, they are most pronounced ahead of the SW front and manifest themselves in the formation of a heated and ionised atmospheric layer (see Fig. 9) due to the radiation from the front. In the consideration of this zone, two characteristic stages of its

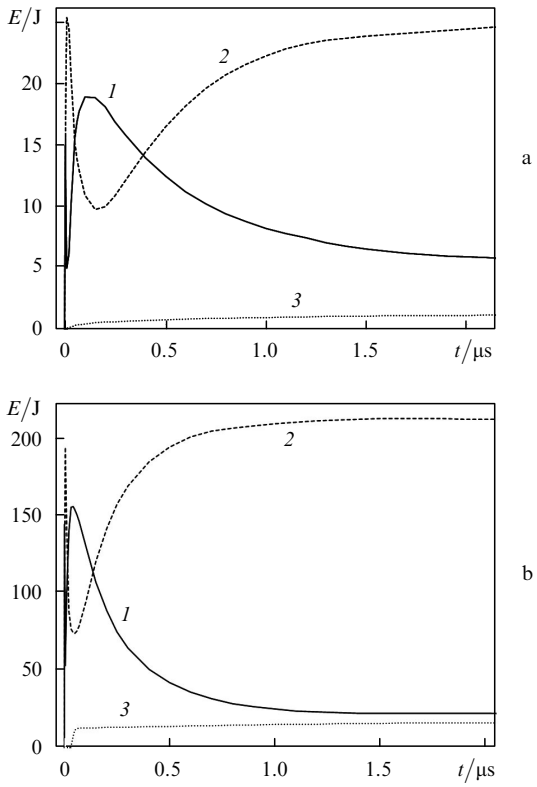

Figure 10. Time dependences of the kinetic (*1*), internal (*2*), and radiated energies (*3*) for the experiments with $E_{las} = 300$ (a) and 2300 J (b).

development may be recognised: at the first stage, the front temperature $T_f > T_{cr}$, where T_{cr} is the critical temperature which characterises the role of radiation in the formation of SW front structure [10]. For the atmospheric density under consideration, its value is equal to 2–3 eV. Referring to Fig. 8a, for $t = 1$ μs [curve (*2*)], $T_f > T_{cr}$ and the front structure is indeed of the form characteristic for super-critical-amplitude waves. For $t = 5$ μs, $T_f < T_{cr}$, to this there corresponds the form of curve (*3*) (the heating zone is hardly visible).

6. Conclusions

The main results of our investigation are as follows:

(i) Experimental data were obtained which permit judging the influence of laser energy deposition (E_{las}) into a spherical target on the parameters of an LPD emerging in its expansion in air (for a pressure of 1 Torr).

(ii) It was shown that these data are adequately described using the physical model and numerical technique set out in Ref. [5].

(iii) Our analysis of the experimental data performed using this approach allows a conclusion that the dependence of the main LPD parameters on E_{las} and t is consistent with the theory of a strong explosion (point-like for $t > 1$ μs). In this case, the plasma behind the SW front turns out to be equilibrium, optically thin, and multiply ionised.

(iv) The main radiation effects reveal themselves in the air ahead of the SW front. They consist in the formation (due to the X-ray target radiation) of an extensive weakly ionised 'halo' and a plasma layer emerging ahead of the front due to the UV radiation emanating from the front. As the (front + layer) structure moves, it changes from supercritical to subcritical.

Subsequently we plan to continue these investigations for other pressures in the chamber with the use of additional diagnostic techniques.

References

1. Bogunenko Yu.D., Bessarab A.V., Bondarenko G.A., et al. *Fiz. Plazmy*, **31**, 1 (2005).
2. Atamanenko V.D., Bessarab A.V., Bondarenko G.A., et al. *Fiz. Plazmy*, **32**, 143 (2006).
3. Annenkov V.I., Bagretsov V.A., Bezuglov V.G., et al. *Kvantovaya Elektron.*, **18**, 536 (1991) [*Sov. J. Quantum Electron.*, **21** (5), 487 (1991)].
4. Dolgoleva G.V. *Voprosy Atomnoi Nauki i Tekhniki. Ser. Metodiki i Programmy Resheniya Zadach Matematicheskoi Fiziki*, (2), 29 (1983).
5. Bel'kov S.A., Dolgoleva G.V. *Voprosy Atomnoi Nauki i Tekhniki. Ser. Matematicheskoe Modelirovanie Fizicheskikh Protsessov*, (1), 59 (1992).
6. Dolgoleva G.V., Zhmailo V.A., Novikova E.A., Statsenko V.P. *Trudy RFYaTs–VNIIEF*, (8), 34 (2005).
7. Gorodnichev A.V., Dolgoleva G.V., Zhmailo V.A., Novikova E.A., Statsenko V.P. *Abstracts of International Workshop on Physics of Compressible Turbulent Mixing* (Cambridge, July 2004).
8. Kravchenko A.G., Litvin D.N., Mis'ko V.V., et al. *Fiz. Plazmy*, **32**, 166 (2006).
9. Bel'kov S.A., Gaiduk S.M., Garanin S.G., Dolgoleva G.V., Kochemasov G.G. *Voprosy Atomnoi Nauki i Tekhniki. Ser. Metodiki i Programmy Resheniya Zadach Matematicheskoi Fiziki*, (1), 76 (1990).
10. Zel'dovich Ya.B., Raizer Yu.P. *Physics of Shock Waves and High-Temperature Hydrodynamic Phenomena, Vols 1 and 2* (New York: Academic Press, 1966, 1967; Moscow: Nauka, 1966).
11. Kuznetsov N.M. *Termodinamicheskie funktsii i udarnye adiabaty vozdukha pri vysokikh temperaturakh* (Thermodynamic Functions and Shock Adiabats of the Air at High Temperatures) (Moscow: Mashinostroenie, 1965).